CHEMISTRY
A EUROPEAN JOURNAL

DOI: 10.1002/chem.200500373

Intramolecular Energy Transfer in Pyrene–Bodipy Molecular Dyads and Triads

Raymond Ziessel,*[a] Christine Goze,[a] Gilles Ulrich,[a] Michèle Césario,[b] Pascal Retailleau,[b] Anthony Harriman,[c] and James P. Rostron[c]

Abstract: Molecules bearing a 4,4-difluoro-8-(aryl)-1,3,5,7-tetramethyl-2,6-diethyl-4-bora-3a,4a-diaza-*s*-indacene (bodipy) core and 1-pyrenyl-1-phenyl-4-(1-ethynylpyrene), or 1-phenyl-4-[1-ethynyl-(6-ethynylpyrene)pyrene] units were constructed in a step-by-step procedure based on palladium(0)-promoted cross-coupling reactions with the required preconstructed modules. X-ray structures of single crystals reveal a twisted arrangement of the two chromophores. In one case, an almost perfect orthogonal arrangement is found. These dyes are strongly luminescent in solution and display rich electrochemistry in which all redox processes of the bodipy and pyrene fragments are clearly resolved. The absorption spectra indicate that the bodipy and pyrene chromophores are spectrally isolated, thereby inducing a large "virtual" Stokes shift. The latter is realised by efficient transfer of intramolecular excitation energy by the Förster dipole–dipole mechanism. The rate of energy transfer depends on the structure of the dual-dye system and decreases as the centre-to-centre separation increases. The energy transfer efficiency, however, exceeds 90% in all cases. The linkage of two pyrene residues by an ethyne group leads to a decrease in the energy-transfer efficiency, with the two polycycles acting as a single chromophore. The directly linked bodipy–pyrene dual dye binds to DNA and operates as an efficient solar concentrator when dispersed in plastic.

Keywords: boron · energy transfer · fluorescent probes · pyrene · redox chemistry

Introduction

The scope and diversity of studies on fluorophores in the realm of the life sciences and biotechnology has continued to expand ever since the initial use of fluorescein, tetramethylrhodamine and phycobiliproteins.[1] One of the more serious problems inherent to most organic fluorescent labels used in biotechnology concerns the relatively small energy gap between the absorption and emission maxima.[2] As a direct consequence of this situation, the sensitivity is reduced because of the need to employ specific filters that discriminate against incident or scattered light. A popular strategy used to enhance the Stokes′ shift, at least in a virtual sense, is to make use of electronic energy transfer between two dyes linked together: here, one dye takes the role of the energy donor (i.e., the absorbing chromophore) and the other operates as the acceptor (i.e., the emitting fluorophore). In many biotechnology applications, the donor and acceptor subunits are connected by aliphatic tethers, which implies a through-space energy-transfer process (i.e., Förster mechanism).[3] Within the framework of this theory, the emission spectrum of the donor must overlap with the absorption spectrum of the acceptor. This requirement places a limit on the "virtual" Stokes′ shift of the dual-dye system. In contrast, through-bond energy transfer offers the possibility to increase the energy separation between absorption and emission maxima, thereby leading to much larger Stokes′ shifts. Indeed, connecting the donor and acceptor subunits by means of unsaturated linkages opens up the possibility to transfer energy by several different routes, such as

[a] Dr. R. Ziessel, C. Goze, Dr. G. Ulrich
Laboratoire de Chimie Moléculaire
École de Chimie, Polymères, Matériaux (ECPM)
Université Louis Pasteur (ULP)
25 rue Becquerel, 67087 Strasbourg Cedex 02 (France)
Fax: (+33) 3-90-24-26-35
E-mail: ziessel@chimie.u-strasbg.fr

[b] Dr. M. Césario, Dr. P. Retailleau
Laboratoire de Cristallochimie, ICSN – CNRS
Bât 27–1 avenue de la Terrasse, 91198 Gif-sur-Yvette, Cedex (France)

[c] Prof. A. Harriman, J. P. Rostron
Molecular Photonics Laboratory, School of Natural Sciences
Bedson Building, University of Newcastle
Newcastle upon Tyne, NE17RU (UK)

Supporting information for this article is available on the WWW under http://www.chemeurj.org/ or from the author.

Dexter-type short-range exchange interactions,[4] excitonic or phonon–phonon-assisted processes and other mechanisms.[5]

A potential way, therefore, to design next-generation molecules suitable for biological fluorescence labelling is to connect a donor component that has strong absorbance at the excitation wavelength to an acceptor that displays a high fluorescence quantum yield. An added requirement is that some type of internal barrier has to be inserted to prevent the donor–acceptor structure acting as a single "supermolecule". This barrier can be imposed by twisting the molecular axis such that the donor and acceptor units are no longer coplanar, since this has the effect of preventing the system from forming an extended LUMO. This deviation from planarity should be kept modest, otherwise through-bond energy transfer might not compete with detrimental non-radiative decay processes.

Among the many stable and strongly luminescent dyes available, 4,4-difluoro-4-bora-3a,4a-diaza-*s*-indacene derivatives (trade name Bodipy[6]) appear to be particularly well suited for the design of new dual-dye systems.[7] In particular, the fluorescence properties of bodipy chromophores can be tailored and tuned by a variety of different substitution patterns on both the pseudo-*meso* position and on the pyrrole ring.[8–10] The availability of sophisticated bodipy-based structures offers the possibility of tackling specific problems linked to: 1) sensing of protons[11] or other cations[12–15] by opto-electronic switching, 2) light-harvesting in porphyrin-based arrays[16] and 3) Stokes shift discrimination in energy transfer based on molecular modules.[17] Their well-established molecular structure makes it easy to establish firm structure–property relationships. For example, with anthracene–bodipy modules, it has been found that both the electrochemical features and the intramolecular energy-transfer processes depend on the nature of the connecting units and on the substitution pattern of the dye.[18]

Recently, we developed a strategy to increase the triplet lifetime of luminescent ruthenium–poly(pyridine) complexes by attaching pyrene (pyr) fragments.[19,20] Pyrene, which is highly fluorescent, absorbs in a region of the spectral range where bodipy is essentially transparent and, as such, might make a useful light harvester. Furthermore, 1-ethynylpyrene appears to be a sufficiently versatile module to merit its attachment to a bodipy residue to form an interesting dual-dye system with a conjugated connector. The availability of 1,6-disubstituted pyrene derivatives suggests that these dual-dye systems could be extended to include dyes with multiple light-harvesting units. In this report, we investigate the synthesis of dual-dye systems comprising a bodipy emitter covalently linked to one or two pyrene absorbers. The photophysical properties of these new systems are described.

Abstract in French: *De nouvelles molécules comprenant un cœur 4,4-difluoro-8-(aryl)-1,3,5,7-tetramethyl-2,6-diethyl-4-bora-3a,4a-diaza-s-indacene (appelé bodipy) et des fragments 1-pyrènyl, 1-phényl-4-(1-éthynylpyrène), ou 1-phényl-4-[1-éthynyl-(6-éthynylpyrène)pyrène] ont été synthétisées par le biais de couplage croisés entre des modules pré-construits. Ces réactions ont été catalysées par du palladium sous-ligandé dans des conditions anaérobiques. Dans deux cas typiques la structure moléculaire déterminée par diffraction aux rayons X sur monocristal révèle un arrangement quasi perpendiculaire des deux sous-unités bodipy et pyrène. L'ensemble des composés sont très fluorescents en solution et dévoilent une voltammétrie cyclique riche en signaux réversibles. L'ensemble des processus d'oxydation et de réduction localisés sur les sous-unité pyrène et bodipy sont bien résolus. De plus ces deux fragments sont spectroscopiquement différenciées ce qui permet d'obtenir des déplacements de Stokes important lorsque la partie pyrène est excitée et que la fluorescence de la partie bodipy est observée. Le processus responsable de ce phénomène est un transfert d'énergie ayant lieu par résonance (mécanisme dit de Förster par interaction dipôle-dipôle). La vitesse de ce transfert d'énergie dépends de la structure moléculaire et décroît en augmentant la distance ente les deux chromophores. L'efficacité de ce transfert est supérieur à 90% dans l'ensemble des cas étudiés. Cependant la connexion par une liaison triple des motifs bodipy et pyrène diminue l'efficacité de ce transfert. La molécule comportant un pyrène directement connecté au bodipy se lie fortement à l'ADN et se comporte comme un concentrateur de photons lorsque dispersé dans des plastiques rigides.*

Results and Discussion

Synthesis of the modules: The simple pyrene-based module **1**, which has a direct connection between the two dyes, was prepared by means of a classical synthetic approach. As outlined in Scheme 1, two equivalents of *kryptopyrrole*[21] and one equivalent of 1-pyrenecarboxaldehyde were allowed to react together under acidic conditions in CH_2Cl_2. The resultant dipyrromethane was oxidised in situ with DDQ. The neutral dipyrromethene compound so formed was deprotonated and treated with boron trifluoride etherate to afford the corresponding bodipy derivative in reasonable yield (25%) for a one-pot synthesis (Scheme 1).

To further extend these studies to modular systems exhibiting significant degrees of electron delocalisation, we sought to employ alkynylene bridges as the means to attach bodipy fragments to pyrene-based chromophores. Initial attention focussed on a bodipy fragment containing a phenyl ring at the *meso* position because this should ensure that the two dyes are tilted with respect to each other. The devised synthetic strategy starts from a prefabricated bodipy unit bearing a reactive C-I function suitable for subsequent cross-coupling reactions with alkynyl pyrene fragments by means of a catalytic reaction promoted by palladium(0). In the first step, the 1-ethynylpyrene building block was synthesised from 1-bromopyrene by a Sonogashira coupling with trimethylsilyl-acetylene, following a literature procedure.[22]

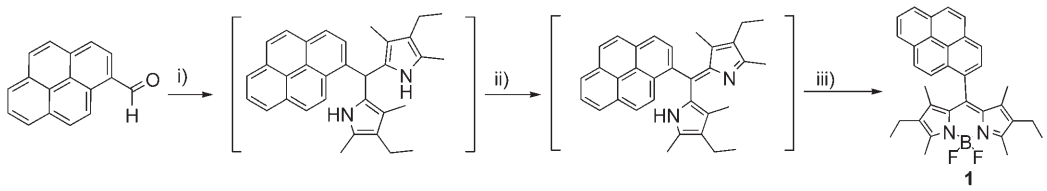

Scheme 1. i) Kryptopyrrole (2 equiv), *p*TsOH cat, CH_2Cl_2; ii) DDQ (1 equiv); iii) TEA (6 equiv), $BF_3{\cdot}Et_2O$ (8 equiv). DDQ = 2,3-dichloro-5,6-dicyano-1,4-benzoquinone, TEA = triethylamine.

A disubstituted pyrene derivative was required for the multi-step synthesis of module **10**. As outlined in Scheme 2, 1,6-dibromopyrene[23] was coupled with one equivalent of methylbutyn-2-ol in the presence of a catalytic amount of $[Pd(PPh_3)_4]$ in *n*-propylamine as the solvent. This protective group was chosen in an attempt to facilitate separation of the desired compound from the starting material and from the disubstituted pyrene on the basis of the polarity imparted by the hydroxy group. Compound **2** was attained in a modest yield (40%) by means of standard chromatography. Related trials with trimethylsilyl protecting groups gave a mixture of three compounds that could not be separated by conventional chromatography. Reversed-phase chromatography was not tried owing to the low solubility of these polyaromatic compounds in polar eluents (water, methanol or acetonitrile). Intermediate **2** was functionalised by means of a second Sonogashira coupling reaction with triethylsilylacetylene to give disubstituted pyrene **3** bearing two protected ethyne functions. The choice of the TES protecting group allowed us to selectively deprotect the isopropyl group in good yield (90%) with NaOH in anhydrous toluene to obtain **4**, without loss of the silyl protective group.[24]

To connect the bodipy acceptor, we made use of the *p*-iodophenyl-bodipy **5** described by Burgess et al.,[7] because reaction conditions for optimised Sonogashira–Heck coupling conditions have been worked out for partially related ethynyl-oligopyridines.[25] Following this improved method, we were able to couple *p*-tolylacetylene, 1-ethynylpyrene and derivative **4** to the aromatic halide **5**, in the presence of $[Pd(PPh_3)_2Cl_2]$/CuI in THF/iPr$_2$NH, in good yields of 93, 85 and 80%, respectively (Scheme 3). The triethylsilyl protecting group of intermediate **8** was removed with K_2CO_3 in a CH_2Cl_2/methanol mixture, to give compound **9** (67%). The final dipyrene-based supermolecule **10** was obtained in excellent yield (95%) by way of a Sonogashira coupling reaction between **9** and 1-bromopyrene, in the presence of a catalytic amount of $[Pd(PPh_3)_4]$ in benzene/iPr$_2$NH.

All new compounds were unambiguously characterised by standard spectroscopic techniques. The ^{1}H NMR spectra display characteristic peaks including two singlets at $\delta \approx 1.3$ and 2.5 ppm for both methylenes and a triplet and quadruplet for the ethyl group of the *kryptopyrrole* subunit. This reflects complete delocalisation of the electrons on the indacene core, leading to two-fold symmetry. In the case of **1**, strong shielding of the methyl group near the pyrenyl unit is observed ($\delta = 0.78$ versus $\delta = 1.31$ ppm for reference compound **5**) owing to its location in the pyrene shielding zone. This situation is favoured by the apparent orthogonality between the two dyes. The *quasi*-aromaticity of the bodipy system is confirmed by the pyrrole quaternary carbon chemical shifts appearing between $\delta = 120$–140 ppm in ^{13}C NMR spectra. In the case of the acetylenic-bridged system, the triple bond appears as two well-defined peaks between $\delta =$ 80–105 ppm. The ^{11}B NMR spectra show a characteristic triplet signal at $\delta = 3.8$–4.0 ppm with a coupling constant of $J \approx 33$ Hz, which is attributed to coupling with two equivalent fluorine nuclei. The FAB$^+$-MS positive-mode mass spectra reveal good stability for these dyes with a major molecular peak corresponding to $[M+H]^+$, followed by fragmentation peaks assigned to the successive loss of fluorine atoms. These observations are in agreement with previous studies on oligopyridine-functionalised bodipy fragments.[25]

Single-crystal X-ray studies: Single-crystal X-ray structures were obtained for compounds **1** and **7**. In both structures, the average B–N and B–F bond lengths are approximately 1.538(8) and 1.393(3) Å, respectively, and the average N-B-N, F-B-F, and N-B-F angles are 107.3(4), 108.6(3) and 110.2(5)°, respectively. As observed previously,[26] pronounced double-bond character is apparent for the C4A–

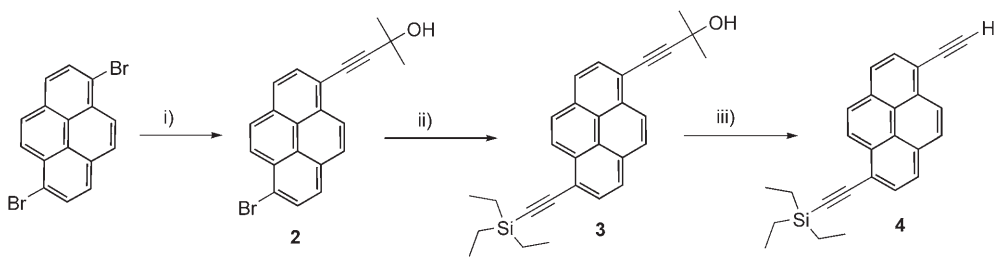

Scheme 2. i) nPrNH$_2$, 2-methylbutyn-2-ol, $[Pd(PPh_3)_4]$, RT; ii) nPrNH$_2$, TES-acetylene, $[Pd(PPh_3)_4]$, RT; iii) toluene, NaOH. TES = triethylsilyl.

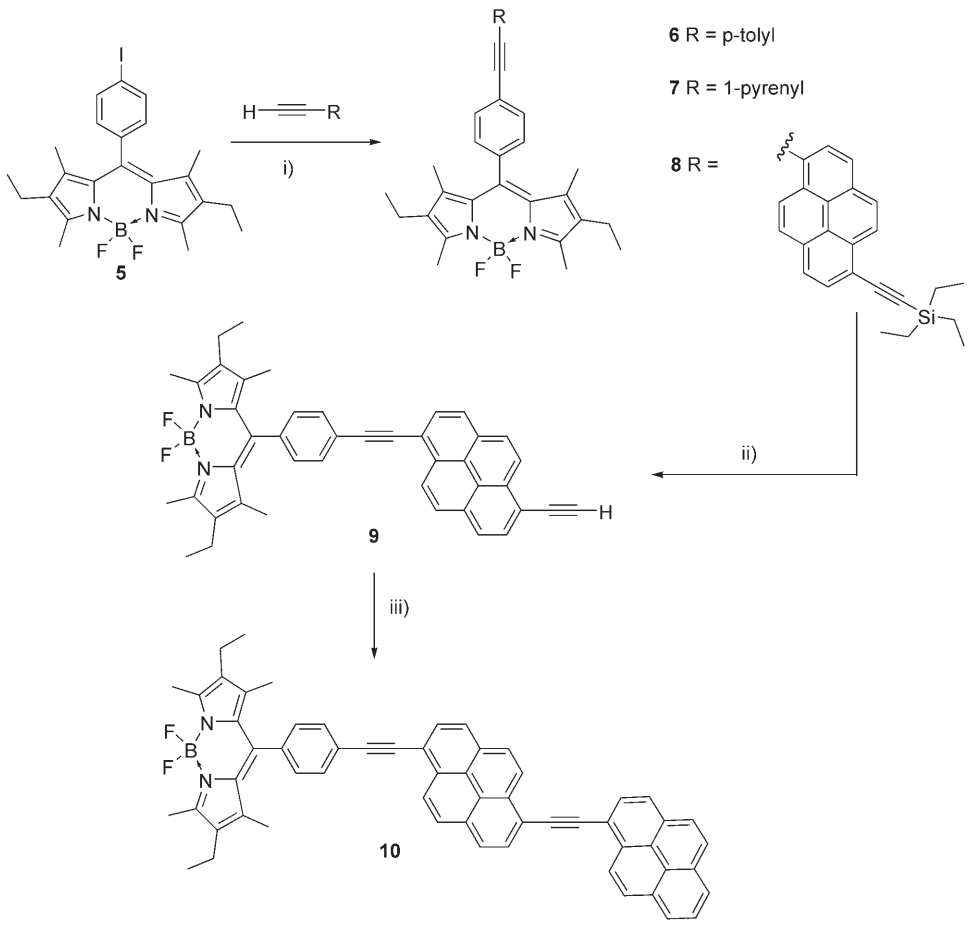

Scheme 3. i) THF/iPr$_2$NH, [Pd(PPh$_3$)$_2$Cl$_2$] (6 mol %), CuI (10 mol %); ii) K_2CO_3, CH_2Cl_2/MeOH; iii) 1-bromopyrene (1 equiv), benzene/iPr$_2$NH, [Pd(PPh$_3$)$_4$] (6 mol %).

N1A and C4B–N1B bonds (1.346(6) Å), but not for the longer C5A–N1A and C5B–N5B bonds (1.398(3) Å). In both compounds, the central six-membered ring lies coplanar with the adjacent five-membered ring (the maximum deviation from the least-squares mean plane for the 12 atoms of the indacene group being 0.025(3) Å). This geometry ensures π-electron delocalisation over the indacene core; however, this does not extend to the two B–N bonds.

The ORTEP view of compound **1** (Figure 1) shows an almost orthogonal geometry between the mean plane of the indacene fragment and the pyrene subunit (dihedral angle 78.3°). The crystal packing diagram shows no special π–π stacking; however, it shows a cofacial arrangement of the pyrene subunit. The shorter distance between two C25 atoms belonging to two neighbouring molecules is 3.595 Å. As shown in Figure 2, the interaction between two neighbouring molecules is less effective than might be expected because of steric constraints imposed by the bodipy fragment. Additionally, it is worth noting that hydrogen bonding is observed between the proton of the co-crystallised nitromethane molecule and the BF_2 fluorine of the bodipy (F2···H1′2 at 2.39 Å, F2–C1′ 3.16 Å, F2-H1′2-C1′ angle = 135.7 °).

A perspective view of compound **7** is shown in Figure 3. The dihedral angle between the mean planes of the pyrene [C19→C34] and the bopidy units [N1A→C5A, N1B→C5B, C10 B] is 29.4°, whilst that between the mean plane of the pyrene group [C19→C34] and the central phenyl ring [C11→C16] is 50.8°. Furthermore, the mean plane between the central aromatic ring [C11→C16] and the bodipy fragment is close to being orthogonal (79.96°). The crystal packing diagram reveals a short separation between the bodipy and pyrene units, these being related centrosymmetrically i[x,y,z] and ii[$-x$,1$-y$,z] with a distance of only 3.644 Å between C15i and C15ii). Likewise, adjacent pyrene rings appear to lie in a cofacial arrangement, centro-symmetrically related, i[x,y,z] and ii, [1$-x$,1$-y$,1$-z$] and separated by only 3.487 Å between C30i and C28ii (Figure 4). Furthermore, the π–π stacked dimers are interlocked in a herringbone arrangement in which hydrogen bonds between aromatic protons (pyrene and phenyl) and BF_2 fluorine is effective: C21-H21···F1 (H···F 2.56 Å, C–F 3.43 Å, C-H-F angle 154.7°), C13-H13···F2 (H···F 2.59 Å, C–F 3.42 Å, C-H-F angle 147.8°), C24-H24···F2 (H···F 2.48 Å, C–F 3.36 Å, C-H-F angle 156.5°). These values are in good agreement with the distances and angles reported for fluoroaromatic compounds.[26]

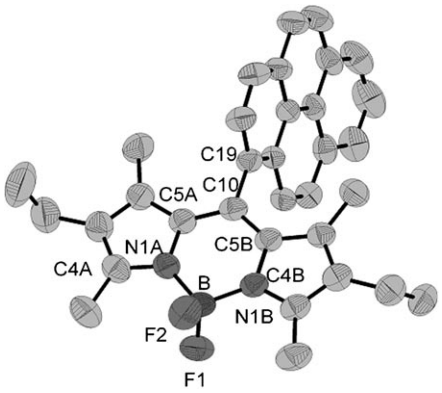

Figure 1. Molecular structure of compound **1** and the atom-labelling scheme. Thermal ellipsoids are plotted at the 30 % level.

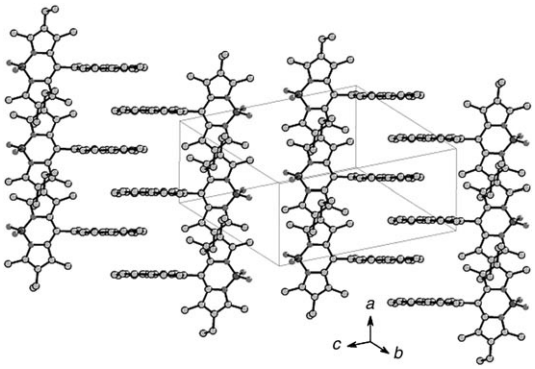

Figure 2. Crystal packing of **1** showing the cofacial arrangement of the pyrene cores along the *a* axis.

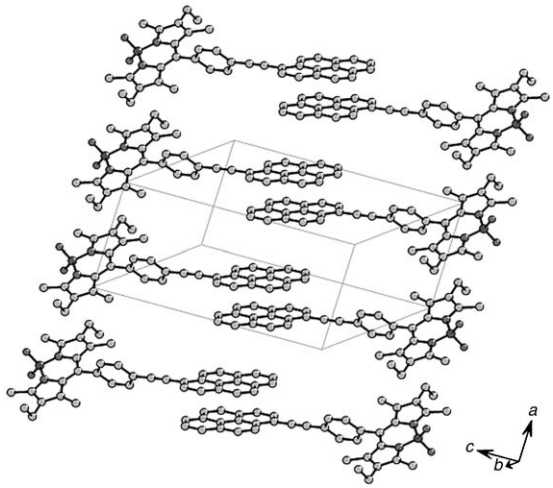

Figure 4. Crystal packing of **7** showing the cofacial arrangement of the pyrene cores along the *a* axis.

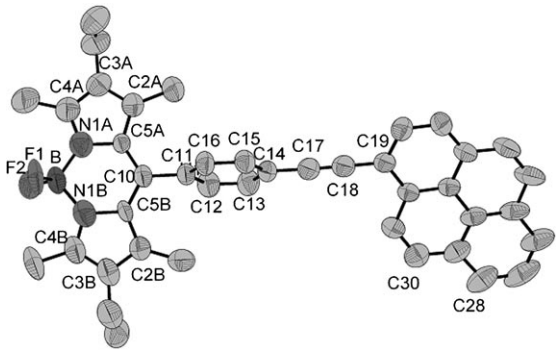

Figure 3. Molecular structure of compound **7** and the atom-labelling scheme. Thermal ellipsoids are plotted at the 30% level.

Molecular modelling studies (see the Supporting Information) are consistent with the X-ray results. Thus, the pyrene-like unit lies orthogonal to the bodipy unit in compounds **1**, **7** and **10**. The bodipy residue is essentially flat in each compound. For **7**, the lowest-energy conformation has the pyrene and phenylene units lying coplanar to each other and orthogonal to the bodipy unit. Likewise, the lowest-energy conformation computed for **10** shows both pyrene rings lying coplanar to the connecting phenylene ring and orthogonal to the bodipy unit. Important bond angles and lengths are comparable to those derived by single-crystal X-ray studies, and there are no obvious indications for strong electronic coupling between the two dyes.

Electrochemical properties: An evaluation of the extent of electronic communication between the various subunits in these dual-dye molecules was made by cyclic voltammetry in CH_2Cl_2 with tetra-*N*-butylammonium hexafluorophosphate as the supporting electrolyte at 20°C. The electrochemical data collected for **1**, **6**–**10** and for some reference compounds (**A**, **B** and **4**, Scheme 4) are gathered in Table 1. The prototypic dye **1** (bodipy-pyrene) displays two reversible, one-electron oxidation waves at +1.02 and +1.48 V vs SSCE and two reversible, one-electron reduction waves at −1.19 and −1.96 V vs SSCE (Figure 5).

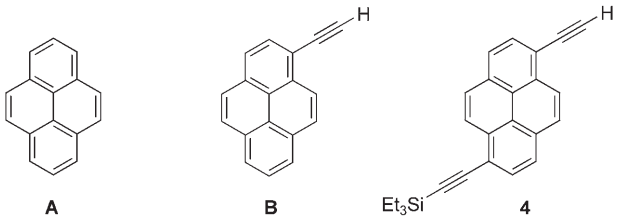

Scheme 4. Reference compounds for the electrochemical measurements.

Table 1. Electrochemical properties of the bodipy-pyrene dyes and reference compounds in solution.[a]

Compound	E^{0}_{ox} [V] (ΔE [mV])		E^{0}_{red} [V] (ΔE [mV])	
	bodipy$^+$/bodipy	pyr$^+$/pyr	bodipy/bodipy$^-$	pyr/pyr$^-$
A	–	+1.34 (irrev, $I_a/I_c \approx 0.2$)	–	–
B	–	+1.30 (irrev, $I_a/I_c \approx 0.3$)	–	–
4	–	+1.36 (irrev, $I_a/I_c \approx 0.2$)	–	−1.78 (90)
1	+1.02 (60)	+1.48 (70)	−1.19 (65)	−1.96 (65)
6	+1.02 (60)	–	−1.20 (65)	–
7	+0.99 (65)	+1.28 (70)	−1.32 (80)	−1.68 (80)
8	+1.00(60)	+1.27 (70)	−1.33 (80)	−1.63 (60)
9	+1.00 (60)	+1.28 (70)	−1.32 (70)	−1.63 (80)
10	+0.99 (70)	+1.24 (70)	−1.35 (70)	−1.70 (80)
				−1.82 (70)

[a] Potentials determined by cyclic voltammetry at 20°C in a deoxygenated CH_2Cl_2 solution containing 0.1 M $TBAPF_6$, at a solute concentration of about 1 mM. Potentials were standardised versus ferrocene (Fc) as an internal reference and converted to SSCE assuming that $E_{1/2}(Fc/Fc^+) = +0.38$ V ($\Delta Ep = 70$ mV) vs SSCE. The error in the half-wave potentials is ±10 mV. Where the redox process is irreversible, the peak potential (E_{ap}) is quoted and the relative peak heights are given as I_a/I_c. All reversible redox steps result from one-electron processes.

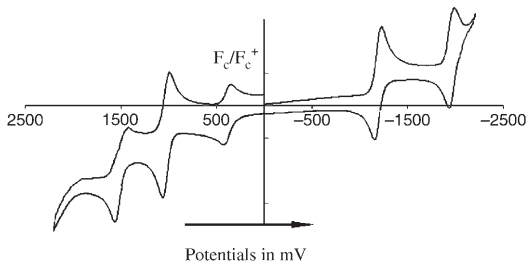

Figure 5. Cyclic voltammetry of compound **1**. Scan rate 200 mV s^{-1}, 0.1 M $TBAPF_6$ in CH_2Cl_2.

By comparison with compound **6** (bodipy-Ph-C≡C-PhCH_3), which lacks the pyrene unit, we can assign the oxidative wave at +1.02 V to a one-electron oxidation of the bodipy unit. Similarly, the first reductive step can be attributed to a one-electron reduction of the bodipy fragment. The measured half-wave potentials are in keeping with results obtained with bodipy-linked poly(pyridine) ligands.[25,27] For the reference compound **6**, no additional redox processes could be detected between +1.6 and −2.2 V versus SSCE. As a consequence, the two additional processes observed for compound **1** at +1.48 V and −1.96 V can be assigned to one-electron oxidation and reduction, respectively, of the pyrene unit.[22]

In **7**, where the pyrene and bodipy units are connected through a -Ph-C≡C- linkage, the oxidation of the bodipy fragment is slightly easier compared to **1**; however, reduction is much harder. A more significant effect is seen for the pyrene fragment in **7**, which becomes easier to both oxidise and reduce than that in **1**. These effects are confirmed by the reduction potentials observed for **8** and **9**. Again, the one-electron oxidation of pyrene is electrochemically reversible. A slight difference is found for **10**, which is equipped with two pyrene residues. Here, there is an additional one-electron reduction step occurring at strongly cathodic potentials. This extra step is presumed to involve attachment of an electron to each of the two pyrene fragments.

Optical properties: Spectroscopic data relevant to the present discussion are collected in Table 2. To clarify interpretation of results obtained with the dual-dye systems, we refer to model compounds **B** and **4** (Scheme 4. With the exception of the phenyl-tolyl derivative **6**, and the pyrene-substituted reference molecules **B** and **4**, all compounds exhibit similar absorption spectral patterns that might be considered characteristic of bodipy linked to pyrene.[7–15] In solution, the absorption spectrum of compound **6** shows a strong $S_0 \rightarrow S_1$ (π–π^*) transition, centered $\lambda \approx 527$ nm with an absorption coefficient of $\approx 60000\ M^{-1}cm^{-1}$, assigned to the bodipy chromophore. The much weaker and relatively broad absorption bands located at $\lambda \approx 357$ nm can be assigned to the $S_0 \rightarrow S_2$ (π–π^*) transition located on the bodipy fragment,[28] whereas the more energetic transition at $\lambda \approx 283$ nm is attributed to the (π–π^*) transition localised on the phenyl-ethynyl subunit. As expected for the 1-ethynylpyrene compound **B**, no absorption is found at $\lambda \approx 530$ nm, but strong π–π^* transitions with a vibronic structure are observed in the 320–370 and 230–310 nm regions.[29]

The grafting of a pyrene unit onto bodipy produces an absorption spectral profile that approximates to a superposition of spectra of the individual components (Figure 6). In addition to the bodipy $S_0 \rightarrow S_1$ (π–π^*) and $S_0 \rightarrow S_2$ (π–π^*) transitions at $\lambda = 528$ and ≈ 370 nm, respectively, three new, broad patterns are seen at ≈ 340, 270 and 230 nm for **1** in methanol. These latter bands are clearly attributable to π–π^* transitions localised on the pyrene subunit. Interestingly, the intensity of the $S_0 \rightarrow S_1$ transition associated with the bodipy unit is increased relative to the reference compound. The absorption spectral profile recorded for **7** remains similar to that found for **1** except for a pronounced broadening of the π–π^* transitions associated with the pyrene-like chromophore (Figure 7). Upon increasing the number of ethyne groups from one to two, the molar absorption coefficient for the pyrene-like chromophore increases from $40000\ M^{-1}cm^{-1}$ in **7** to $60000\ M^{-1}cm^{-1}$ in **8** and **9**. For **10**, the presence of two pyrene-like units results in a set of intense transitions in the range $\lambda = 340$ to 480 nm (Figure 8). These bands are clearly associated with the pyrene-like chromophore; however, it is not obvious whether this unit acts as a single giant chromophore or as two sep-

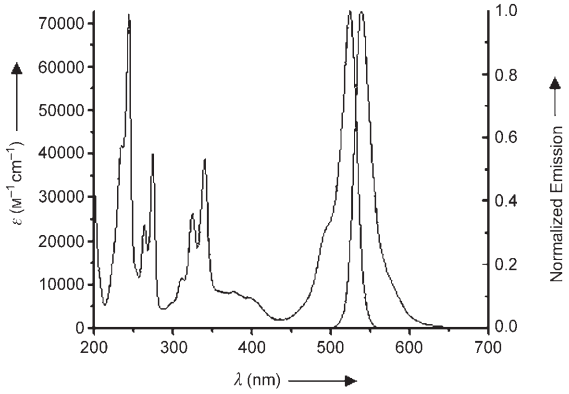

Figure 6. Overlay of absorption and fluorescence spectra recorded for **1** in methanol solution.

Table 2. Photophysical properties and the results of emission spectral fitting for the various dual-dyes in methanol solution.

Property	**1**	**7**	**10**
Φ_F	0.9	0.70	0.63
τ_S[ns^{-1}]	7.0	4.0	4.0
$k_{RAD}/10^8$[s^{-1}]	1.3	1.8	1.6
$k_{NR}/10^7$[s^{-1}]	1.4	7.5	9.3
ΔE[cm^{-1}]	18600	18600	18600
$h\omega_M$[cm^{-1}]	1370	1480	1500
$h\omega_L$[cm^{-1}]	685	740	750
γ	1.52	1.50	1.50
S_M	0.22	0.21	0.20
ε[$M^{-1}cm^{-1}$][a]	73000	60000	58000
λ_{max}[nm^{-1}][b]	524	523	523

[a] Molar absorption coefficient measured for the peak of the bodipy S_0–S_1 transition. [b] Absorption maximum.

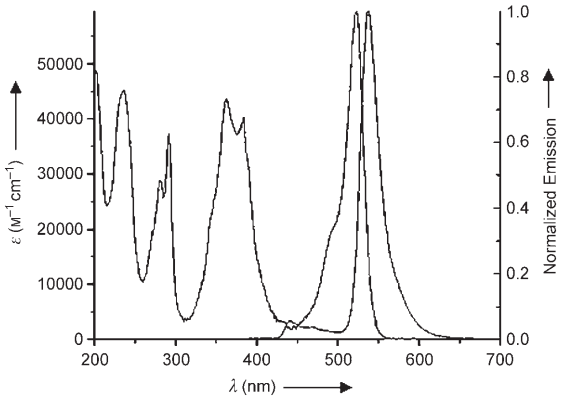

Figure 7. Overlay of absorption and fluorescence spectra recorded for **7** in methanol solution.

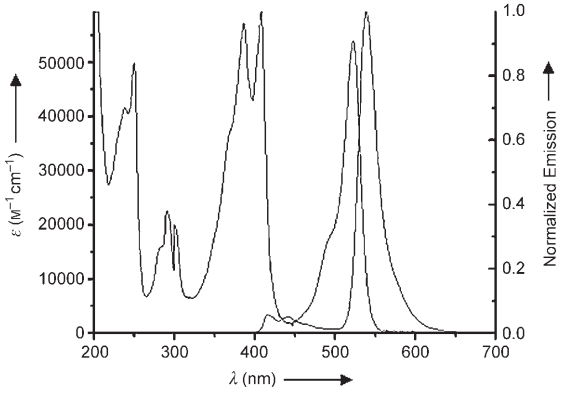

Figure 8. Overlay of absorption and fluorescence spectra recorded for **10** in methanol solution.

arate units. In this case, the absorption coefficient of the strongest band is superior to the bodipy $S_0 \rightarrow S_1$ (π–π^*) transition. Finally, no charge-transfer (CT) absorption bands are evident at long wavelengths for these neutral compounds as is often observed in other organic fluorophores in polar solvents.[30,31]

The fluorescence properties were examined under ambient conditions in a very dilute methanol solution. Fluorescence from the bodipy unit is apparent in all the compounds studied (Figures 6–8). This emission profile shows good mirror symmetry with the corresponding absorption band and displays a small Stokes shift of $\approx 600\,cm^{-1}$. The measured fluorescence quantum yields (Φ_F) are high under these conditions and are little affected by the presence of dissolved molecular oxygen. Emission from the bodipy unit decays with first-order kinetics and a lifetime (τ_S) in the order of 4–7 ns (Table 2). The fluorescence spectral profiles for **1** and **7** were found to be unaffected by cooling the solution to the freezing point. No phosphorescence could be detected at 77 K and the overall change in Φ_F on cooling from 298 to 77 K was less than 10%. These photophysical properties are in accordance with those reported for somewhat related boron-dipyrromethene dyes.[32] It is interesting to note, however, that both Φ_F and τ_S are reduced for **7** and **10** relative to **1** (Table 2). This effect can be traced to an increase in the rate of non-radiative decay (k_{NR}) for the compounds bearing an ethynyl group because the radiative rates (k_{RAD}) are little affected by substitution. Similar behaviour is observed in CH_2Cl_2 solution (Table 3).

Table 3. Spectroscopic data for the compounds in CH_2Cl_2 at 298 K.

Compound	λ_{abs} [nm]	ε [$M^{-1}cm^{-1}$]	λ_F [nm]	Φ_F[a]	τ_F [$10^8\,s^{-1}$]	k_{RAD} [$10^7\,s^{-1}$]	k_{NR}
1	528	83000	544	0.90	7.0	1.3	1.4
6	527	56000	549	0.87	5.5	1.6	2.4
7	526	60000	544	0.60	5.0	1.2	8.0
8	529	69000	544	0.82	5.1	1.6	3.5
9	527	66300	542	0.95	5.2	1.8	0.96
10	532	52900	545	0.68	4.3	1.6	7.4

[a] With Rhodamine 6G, as reference $\Phi = 0.78$ in water, $\lambda_{exc} = 488$ nm.[36] All Φ_F are corrected for changes in the refractive index.

Deactivation of the S_1 state localised on the bodipy unit can be considered within the framework of the Englman–Jortner energy-gap law [Eq. (1)] within the weak coupling limit.[33] Here, the rate constant for non-radiative decay (k_{NR}) is related to the energy gap between emitting and ground states (ΔE) and the magnitude of a medium-frequency vibrational mode ($h\omega_M$) coupled to the decay process. For the dyes under consideration here, there is no change in the energy gap ($\Delta E = 18600\,cm^{-1}$) whilst curve-fitting analyses of the fluorescence spectral profiles indicated that the value of $h\omega_M$ is surprisingly sensitive to the nature of the emitter (Table 2). The derived values refer to C=C and/or C=N stretching vibrations. For **1**, **7** and **10**, the emission profiles also indicate the involvement of a low-frequency vibrational mode ($h\omega_L$) that couples to the decay process. This latter process probably refers to twisting of the aryl group attached directly to the bodipy unit. The Huang–Rhys factors (S_M) are closely comparable for the various compounds, as evidenced from the fact that the emission spectra and Stokes shifts are very similar throughout the series. The parameter γ, as defined by Equation (2), contains pertinent structural information concerning the relative displacement of the potential energy surfaces for the ground and excited states. Here, d refers to the number of degenerate, or almost degenerate, vibrational modes of frequency $h\omega_M$, and Δ_M is the reduced displacement of that mode. There is, however, little variation in this term upon substitution. The variation in $h\omega_M$ gives a quantitative explanation of the observed changes in k_{NR}. Thus, small changes in the vibrational pattern result in observable perturbation of the emission yield and lifetime.

$$k_{NR} = \frac{C^2\sqrt{2\pi}}{\hbar\sqrt{h\omega_M \Delta E}} \exp(-S_M) \exp\left\{-\frac{\gamma \Delta E}{h\omega_M}\right\} \quad (1)$$

$$\gamma = \ln\left(\frac{\Delta E}{d h\omega_M \Delta_M^2}\right) - 1 \quad (2)$$

For the directly linked dual-dye **1**, the fluorescence excitation spectrum was found to exactly match the absorption spectrum recorded over the entire spectral range (see the Supporting Information). In particular, photons absorbed by the pyrene-like subunit are channelled to the bodipy unit with high efficiency. No fluorescence could be detected from the pyrene-like unit within the range $\lambda = 350$–500 nm. If the fluorescence quantum yield and singlet lifetime for pyrene under these conditions are taken to be 0.76 and 140 ns, respectively, it is clear that the excited singlet state resident on the pyrene substituent in **1** is quenched by a factor of at least 100-fold. This suggests that the rate constant for intramolecular excitation energy transfer (k_F) for **1** is $>10^{10}\,s^{-1}$. This rate constant is essentially independent of temperature over the range 77–293 K.

For both **7** and **10**, it was noted that direct excitation into the pyrene-like subunit resulted in the appearance of weak fluorescence at approximately 400–500 nm (Figure 7 and Figure 8). This latter emission is characteristic of fluorescence from an ethynylated pyrene derivative. Indeed, the corrected excitation spectrum recorded for this emission profile remained in excellent agreement with the absorption profile attributed to the pyrene-like unit. Excitation spectra recorded for emission from the bodipy unit were consistent with fast energy transfer from the pyrene-like fragment; a comparison of the absorption and excitation spectra over the region of interest shows that intramolecular energy transfer occurs with an efficiency of ≈ 95 and 90%, respectively, for **7** and **10** (see the Supporting Information). The energy-transfer efficiency measured for **7** is essentially independent of the temperature over the range 77 to 293 K. A comparison of the quantum yields of pyrene-like fluorescence with those measured for appropriate reference compounds supports the concept of efficient intramolecular energy transfer in **7** and **10**. These latter experiments indicate that the energy-transfer efficiency exceeds 90% for both **7** and **10**. On the basis of the values of the ethyne-linked pyrene dimer **C** as a reference ($\Phi_F = 0.78$, $\tau_S = 1.5$ ns), it is concluded that the energy-transfer rates for **7** and **10** are in the order of $3.0\times10^{10}\,s^{-1}$ and $7\times10^{9}\,s^{-1}$, respectively.

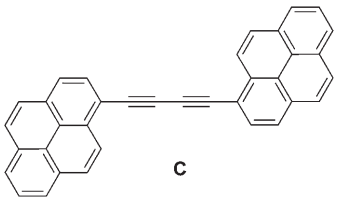

C

It is instructive to closely examine the excitation and absorption spectra recorded for **10** (Figure 9). Although energy transfer is not quite complete in this system, the spectral profiles are closely comparable. This finding suggests that the two pyrene subunits act as a single giant chromophore rather than as two separate species. Support for

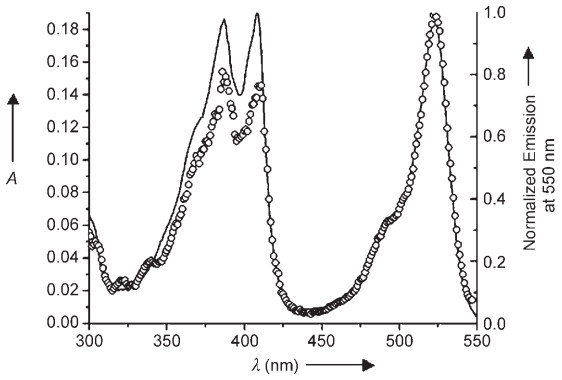

Figure 9. Comparison of absorption (——) and excitation (○) spectra recorded for **10** in methanol solution.

this notion comes from quantum-chemical computations made on the lowest-energy conformation (see the Supporting Information). Thus, calculations indicate that both the LUMO and HOMO for **1** are localised on the bodipy unit with LUMO(−1) and HOMO(1) being centered on the pyrene residue. This situation is consistent with the results from optical studies, namely, the lowest-energy excited state is associated with the bodipy unit. The excited singlet state localised on the pyrene-like nucleus lies at much higher energy. Similar calculations made for **7** again indicate that both the LUMO and HOMO reside on the bodipy residue. The pyrene-like unit is clearly associated with LUMO(−1) and HOMO(1); however, whilst these latter orbitals involve the ethynyl group, they do not encompass the phenylene ring. As such, the two dyes are isolated in electronic terms. For the extended system **10**, the calculations indicate that both LUMO and HOMO are localised on the bodipy residue, without penetrating onto the linking phenylene ring. It is clear that HOMO(1) is delocalised over both pyrene polycycles and over the two ethyne groups. The electron density is evenly distributed over the two polycycles, but not on the bridging phenylene ring. Again, this finding indicates that the two dyes are electronically decoupled. At the same time, LUMO(−1) is spread asymmetrically over both pyrene residues and the attached ethynes. Unlike HOMO(1), the electron density is somewhat localised on the central pyrene fragment, but it does include the distal pyrene. We can safely conclude, therefore, that the two pyrene residues act cooperatively as a single chromophore and that the corresponding S_1 state is delocalised over the entire substituent.

These quantum-chemical computations, together with the photophysical properties recorded for the bodipy fragments in compounds **1**, **7** and **10** indicate that the two dyes are not in strong electronic communication. This is presumably a consequence of their orthogonal geometries. The two dyes, however, are in quite close proximity such that electronic energy transfer might take place by way of the Förster dipole–dipole mechanism.[34] Here, the rate constant for energy transfer (k_{ET}) is related to the centre-to-centre separation distance (R_{CC}), the refractive index of the surrounding medium (n), a spectral overlap integral (J_F), an orienta-

tion factor (K), and the photophysical properties of the donor according to Equation (3). The latter information was collected for appropriate pyrene-based molecular fragments in deoxygenated methanol at room temperature. The overlap integral was then calculated for emission from the pyrene-based fragments and absorption by the relevant bodipy unit in the dual-dye compounds. The separation distance was determined from the energy-minimised conformations (see the Supporting Information). These latter structures were also used to compute the orientation factors using calculated transition dipoles. The derived values are compiled in Table 4, together with the computed rate constants.

Table 4. Virtual Stokes shifts and parameters associated with intramolecular energy transfer in methanol solution.

Parameter	**1**	**7**	**10**
Stokes shift [cm^{-1}]	10900	7400	3700
J_F [10^{-14} mol^{-1} cm^6][a]	2.2	0.096	0.092
K^2[b]	3.1	2.0	2.0
τ_D [ns^{-1}][c]	140	1.5	1.5
Φ_F[d]	0.76	0.78	0.78
R_{CC} [Å^{-1}]	7.3	14.1	18.8
k_F [10^9 s^{-1}]	670	37	6.2
P_{ET} [%][e]	100	95	90

[a] Spectral overlap integral calculated for the reference compounds. [b] Orientation factor computed from the energy-minimised structures. [c] Excited singlet lifetime of the pyrene-like donor. [d] Fluorescence quantum yield of the pyrene-like donor. [e] Energy-transfer efficiency calculated from the excitation spectra.

$$k_F = \frac{8.8 \times 10^{-25} \Phi_F K^2 J_F}{n^4 \tau_D R^6_{CC}} \quad (3)$$

For **1**, the calculated k_F value is 6.7×10^{11} s^{-1} and is consistent with the absence of fluorescence from the pyrene residue. The close proximity of the reactants, despite their orthogonality, favours very fast energy transfer. If, under these conditions, pyrene is taken as having a fluorescence lifetime of 140 ns, it appears that the probability of fluorescence quenching is unitary. This situation is favoured by the excellent overlap between S_0–S_2 absorption in bodipy and fluorescence from pyrene. The increased separation for **7**, together with the modified photophysical properties of the reference compound and the reduced spectral overlap, decrease the calculated k_F to 3.7×10^{10} s^{-1}. Here, the fluorescence lifetime of the pyrene model compound is only 1.5 ns and the energy-transfer efficiency is about 95%. The inherent Φ_F for the pyrene model is comparable to that of the bodipy unit so it is not too surprising that a small amount of residual fluorescence is seen from the pyrene unit in **7**. Indeed, on the basis of the calculated k_F value, the estimated Φ_F for pyrene-like fluorescence from **7** becomes 0.014. The projected lifetime of 27 ps for the pyrene-like fluorescence is below the temporal resolution of our instrument. It should be noted that the ethynyl substituent pushes the pyrene-like fluorescence towards higher energy than the S_0–S_2 absorption band on the bodipy unit. This reduces both the overlap integral and the virtual Stokes shift (Table 4).

For **10**, the overlap integral and orientation factor remain comparable to those measured for **7**, although there is a marked decrease in the average separation distance (Table 4). The latter situation arises because the two pyrene polycycles are assumed to function as a single giant chromophore so that the calculated k_F becomes 6.2×10^9 s^{-1}, which translates to an energy-transfer efficiency of about 91%. This is consistent with the excitation spectrum, where the energy-transfer efficiency is about 90%; however, it has to be realised that there is considerable uncertainty about the size of the separation distance. The expected Φ_F for the pyrene-like unit is 0.08 which, again, is in reasonable agreement with the experimental result.

Conclusion

Highly fluorescent and soluble dual-dye probes have been synthesised by a strategy that combines the advantages of readily available starting materials with the synthetic efficiency of C–C bond formation promoted by palladium(0) catalysts. A straightforward route allows the coupling of a disubstituted pyrene unit in which one alkyne function is protected by a trimethylsilyl group. After deprotection and cross-coupling to a second pyrene entity, an extended dual-dye system is produced that has greatly increased absorptivity in the λ = 400–500 nm region. Each of the three dual-dye systems examined here exhibits efficient intramolecular excitation energy transfer from pyrene to bodipy. The latter unit fluoresces strongly, even in aerated solutions at room temperature. Several important considerations can now be raised regarding these systems. Firstly, direct linkage of the pyrene and bodipy units in an orthogonal arrangement leads to the largest virtual Stokes shift of 10900 cm^{-1} and retains the best photophysical properties for the emitter. Energy transfer is quantitative and very fast because of an improved spectral overlap integral. However, absorption by the pyrene-like chromophore is modest. Secondly, connection of the two dyes through a phenylethyne linker has the effect of reducing the energy-transfer efficiency and lowering the fluorescence yield and lifetime of the emitter. There is also a reduction in the virtual Stokes shift to 7400 cm^{-1}. However, absorptivity in the near-UV region is increased significantly. Thirdly, these latter effects are amplified by joining a second pyrene to the first pyrene unit. Here, the two pyrene units cooperate to form a giant chromophore that is less effective at transferring excitation energy to the terminal bodipy unit. The virtual Stokes shift drops to 3700 cm^{-1}, but there is a further increase in absorptivity in the near-UV region.

These dual-dye systems are photostable in solution and do not form a triplet excited state in a measurable yield. Fluorescence yields are high and there are no indications for aggregation in solution. Because the dyes are neutral, they dissolve in a wide range of common organic solvents, but not in water. The orthogonal geometry keeps the two dyes in electronic isolation. It is interesting to note that com-

pound **10** has high absorptivity between 350 and 450 nm. This compound also shows dual fluorescence, with emission bands at both 450 and 550 nm. The emitting states are too far apart in energy for them to lie in thermal equilibrium. For all three dual-dye systems, the energy-transfer efficiency and the photophysics of the emitter are essentially independent of temperature. The Förster mechanism is insensitive to changes in solvent polarity. As a consequence, the new dyes described here appear to be robust and versatile fluorescent tags that display relatively large virtual Stokes shifts.

It was observed that **1**, in particular, dispersed readily into poly(methylmethacrylate) (PMMA) to form a highly fluorescent plastic film. Dried films standing in room light were stable over one year without apparent loss of fluorescence. The absorption and emission spectra remain comparable to those recorded for methanol solutions and it is clear that the fluorescence quantum yield for the PMMA-dispersed dye is very high. The fluorescence lifetime was recorded as 6.6 ns and is only slightly affected by changes in temperature. Because the absorption spectrum retains the well-resolved fine structure associated with the pyrene-like unit, ratiometric fluorescence measurements can be made. Also, the films display high internal reflection, which indicates that they would be excellent solar concentrators. Films prepared from **10**, with the increased absorptivity in the 350–450 nm range, indicates that they would be enhanced solar concentrators.[37]

Finally, samples of **1** were incubated with calf-thymus DNA in water (pH 7, $I = 0.05$ M) at room temperature. Little fluorescence could be observed until after saturation of the duplex with dye. At this point, free dye in the solution shows strong fluorescence. Although no evidence was sought as to the mode of association between **1** and DNA, it is clear that complexation occurs and leads to fluorescence quenching. On the basis of spectrophotometric titrations (see the Supporting Information), it was concluded that **1** occupies two base pairs in the association step. It is known that pyrene residues intercalate into double-stranded DNA and undergo electron transfer with the individual nucleic acid bases, especially cytosine.[38] Illumination of the pyrene subunit of **1**, therefore, after complexation with DNA could result in rapid electron transfer to cytosine, in competition to energy transfer to bodipy. The reduction potentials are such that the resultant pyrene radical cation would oxidise the bodipy unit. Of course, electron transfer would need to be very fast; however, it is known that this occurs with intercalated reagents. Illumination of the bodipy unit of DNA-bound **1** also fails to give fluorescence from the dye. It is considered unlikely that the bodipy unit intercalates into the strand, but association must position the dye close to the nucleic acid bases. As such, light-induced electron transfer between bodipy and guanine is a possible cause of the extinguished fluorescence. At low concentrations of dye, this behaviour indicates that it would be a very sensitive fluorescent sensor for double-stranded DNA.

Experimental Section

General methods: The 200.1 (^{1}H), 300.1 (^{1}H), 400 (^{1}H), 50.3 (^{13}C), 75.46 (^{13}C) and 100.3(^{13}C) MHz NMR spectra were recorded at room temperature with perdeuterated solvents as the internal standard: δ(H) is given relative to residual protiated solvent; δ(C) is given relative to the solvent. The 128.4 MHz ^{11}B NMR spectra were recorded at room temperature with glass residual B_2O_3 as the reference. A fast-atom bombardment ZAB-HF-VB-analytical mass spectrometer operated in the positive mode was used with *m*-nitrobenzyl alcohol (*m*-NBA) as the matrix. FT-IR spectra were recorded for the neat liquid or as a thin film, prepared with a drop of CH_2Cl_2 and evaporated to dryness on KBr pellets. Melting points were obtained with a capillary melting point apparatus in open-ended capillaries and are uncorrected. Chromatographic purification was conducted with standardised Al_2O_3 (grade 90). Thin-layer chromatography (TLC) was carried out on Al_2O_3 plates coated with fluorescent indicator. All solvent mixtures are given as volume/volume ratios.

Materials: CH_2Cl_2 and iPr$_2$NH, were distilled from P_2O_5 and KOH, respectively. Kryptopyrrole, 1-pyrenecarboxaldehyde, 1-bromopyrene, trimethylsilylacetylene, KF, DDQ, $BF_3{\cdot}Et_2O$, *p*TsOH and Et_3N were obtained from commercial sources and used without further treatment. Samples of $[Pd(PPh_3)_2Cl_2]$[39] and $[Pd(PPh_3)_4]$.[40] were prepared and purified according to literature procedures. Samples of $[Pd(PPh_3)_2Cl_2]$ was recrystallised from DMSO. All reactions were carried out under dry argon using Schlenk-tube and vacuum-line techniques.

Spectroscopic measurements: Absorption spectra were recorded with a Hitachi U3310 spectrophotometer whilst emission spectra were recorded with a Hitachi F4500 spectrophotometer. All studies were made at 20 °C unless stated otherwise. Excitation and emission spectra were fully corrected by reference to a standard lamp. Solutions were deoxygenated by purging with dried N_2 prior to recording the spectrum. Fluorescence quantum yields were measured relative to Rhodamine 6G in methanol. Fluorescence lifetimes were measured with a Ivon–Jobin fluorolog tau-3 spectrometer in dilute solutions. Decay profiles were deconvoluted from the instrument response function before analysis. The spectral curves were fitted with PeakFit. Spectral overlap integrals were calculated by standard methods and appropriate reference compounds in dilute methanol solutions. Variable-temperature studies were conducted with an Oxford Instruments Optistat DN cryostat.

Electrochemical measurements: Electrochemical studies employed cyclic voltammetry with a conventional 3-electrode system and a BAS CV-50W voltammetric analyzer equipped with a Pt microdisk (2 mm^2) working electrode and a silver wire counter-electrode. Ferrocene was used as an internal standard and was calibrated against a saturated calomel reference electrode (SSCE) that was separated from the electrolysis cell by a glass frit presoaked in electrolyte solution. Solutions containing the electro-active substrate in deoxygenated, anhydrous CH_2Cl_2 with doubly recrystallised tetra-*n*-butylammonium hexafluorophosphate (0.1 M) as the supporting electrolyte. The quoted half-wave potentials were reproducible within about 20 mV.

X-ray crystal structure determinations of compound 1 and 7: The X-ray diffraction data were recorded at ambient temperature on an Enraf-Nonius Kappa-CCD diffractometer with graphite-monochromated $Mo_{K\alpha}$ radiation ($\lambda = 0.71073$ Å), from a very thin, red plate-type crystal ($0.500\times0.180\times0.025$) for **1** and from a dark red prism ($0.45\times0.40\times0.30$ mm) for **7**. A ϕ scan with an increment of 1.6° over 183° was recorded and completed by three subsequent ω-scans for crystal **1**, which belongs to triclinic space group, $P\bar{1}$. A full sphere of data was collected by ϕ-axis rotation with an increment of 2° for **7**, in the monoclinic space group, $P2_1/c$. "Dezingering" was accomplished by measuring each frame twice with 180 s exposure per degree for **1** and 25 s exposure per degree for **7**. Data reductions were carried out with the DENZO program from the HKL suite.[41] This allowed the integration of reflections up to $\theta = 23.3°$, which were subsequently reduced to 4185 independent reflections ($R_{merge} = 0.038$) for **1**, whereas 7351 unique reflections up to $\theta = 27.5°$ were measured for **7**. The structures were solved by direct methods (SHELX-S)[42] and all non-hydrogen atoms were refined with anisotropic displacement parameters using SHELX-L[42] by full-matrix least-squares

on F^2 values. All hydrogen atoms were located on difference-Fourier syntheses and were refined with a riding model and with U_{iso} set to 1.15 times that of the attached C-atom (= 1.2 for the methyl group).

In each case, the asymmetric unit consists of one ligand compound and one co-crystallised solvent molecule (a nitromethane molecule in **1** and a CH_2Cl_2 molecule in **7**). The largest difference peak and hole (0.705 and −0.475 e Å^{-3}) in **1** is in agreement with the disordered nitromethane molecule. The CH_2Cl_2 molecule is also affected by disorder in **7**. Two positions were found on the difference Fourier syntheses. Better convergence was obtained with an occupancy factor of 0.50. For **1**, the final conventional R value is 0.0740 for 2784 observed reflections with $F_o > 4\sigma(F_o)$ and 381 parameters, and 0.1091 for all data, $wR(F^2) = 0.23$ for all, $w = 1/[\sigma^2(F_o)^2 + (0.1192P)^2 + 1.0874P]$, where P = $(F_o^2 + 2F_c^2)/3$. For **7**, the final conventional R is 0.0842 for 4132 $F_o > 4\sigma(Fo)$, 468 parameters and 4 restraints, and 0.141 for all data, $wR(F^2) = 0.28$ for all, $w = 1/[\sigma^2(F_o)^2 + (0.1373P)^2 + 2.4515P]$ where $P = (F_o^2 + 2F_c^2)/3$. The largest difference peak and hole are 0.4 and −0.4 e Å^{-3}. A summary of the crystallographic data is given in Table 5.

Table 5. Summary of crystal data, intensity measurements and structure refinement for **1** and **7**.

	1	**7**
formula	$C_{33}H_{31}BF_2N_2{\cdot}CH_3NO_2$	$C_{41}H_{35}BF_2N_2{\cdot}CH_2Cl_2$
M_r	565.45	687.43
crystal system	triclinic	monoclinic
space group	$P\bar{1}$	$P2_1/c$
a [Å]	7.266(4)	7.940(3)
b [Å]	12.168(3)	26.19 (1)
c [Å]	17.628(4)	17.024(7)
α [°]	100.33 (2)	90.00
β [°]	90.79 (2)	94.062(4)
γ [°]	104.64 (2)	90.00
V [Å^3]	1480.6(10)	3531(2)
λ [Å]	0.71073	0.71073
$F(000)$	596	1432
ρ_{calcd} [Mg m^{-3}]	1.268	1.293
μ [mm^{-1}]	0.087	0.228
crystal size [mm]	0.500 × 0.180 × 0.025	0.450 × 0.400 × 0.300
T [K]	293(2)	293(2)
reflections collected/ unique	10525/4185	14238/7351
θ range [°] (completeness)	2.35 < θ < 23.24 (98.5 %)	1.43 < θ < 27.48 (100 %)
hkl range	−8/8, −13/13, −19/19	−10/10, −33/34, −20/20
refined data/obs. $I > 2\sigma(I)$	4181/2784	7347/4132
restraints/parameters	3/381	4/468
goodness-of-fit on F^2	1.059	1.022
final R indices	$R1 = 0.0740$	$R1 = 0.0842$
$[I > 2\sigma(I)]$	$wR2 = 0.2070$	$wR2 = 0.2332$
R indices (all data)	$R1 = 0.1091$	$R1 = 0.1414$
	$wR2 = 0.2367$	$wR2 = 0.2861$
max. Fourier diff. [e Å^{-3}]	0.705, −0.475	0.48, −0.36

CCDC-263269 (**1**) and CCDC-263270 (**7**) contain the supplementary crystallographic data for this paper. These data can be obtained free of charge from the Cambridge Crystallographic Data Centre via www.ccdc.cam.ac.uk/data_request/cif. deposit@ccdc.cam.uk).

4,4-Difluoro-8-(1-pyrenyl)-1,3,5,7-tetramethyl-2,4-diethyl-4-bora-3a,4a-diaza-*s*-indacene (1): To a solution of kryptopyrrole (0.65 mL, 4.8 mmol) in anhydrous CH_2Cl_2 (150 mL) was added pyrene-1-carboxaldehyde (0.5 g, 2.17 mmol) and a catalytic amount of *p*TsOH. This mixture was stirred for four days at room temperature. DDQ (0.55 g, 2.5 mmol) was added, and the mixture was stirred for 4 h. Triethylamine (1.8 mL, 13 mmol) and $BF_3{\cdot}Et_2O$ (2.2 mL, 17.4 mmol) were added to the deep red solution, which turned pink with glints of green, and was stirred for one more day. The solution was washed with aqueous $NaHCO_3$ solution and the organic layer was dried over $MgSO_4$. Column chromatography (alumina; CH_2Cl_2/hexane, gradient 2:8 to 3:7) followed by recrystallisation from CH_2Cl_2/hexane gave the desired compound. Yield: 0.28 g (25 %); ^{1}H NMR ($CDCl_3$, 300 MHz): δ = 8.02–8.29 (m, 8H), 7.89 (d, 1H, ^3J = 7.7 Hz), 2.60 (s, 6H), 2.23 (q, 4H, ^3J = 7.5 Hz), 0.92 (t, 6H, ^3J = 7.5 Hz), 0.78 ppm (s, 6H); ^{13}C{^{1}H} NMR ($CDCl_3$, 300 MHz): δ = 153.9, 138.9, 138.5, 132.8, 131.6, 131.3, 131.1, 130.3, 129.5, 128.7, 128.2, 127.3, 126.4, 126.2, 125.6, 125.5, 125.3, 124.6, 124.5, 124.4, 17.4, 14.6, 12.6 , 11.1 ppm; ^{11}B NMR ($CDCl_3$, 400 MHz): δ = 4.08 ppm (t, J(B,F) = 33.7 Hz); UV/Vis (CH_2Cl_2): λ (ε [M^{-1}cm^{-1}]) = 529 (83000), 342 (45600), 327 (30100), 276 (48300), 265 (29500), 245 (82000) nm; FT-IR (KBr): $\tilde{\nu}$ = 2961 (s), 2205 (s), 1598 (s), 1540 (s), 1474 (s), 1320 (s), 1191 (s), 1070 (s), 979 (s), 846 (s) cm^{-1}; FAB$^+$/MS (*m*NBA): *m*/*z* (%): 505.2 (100) [*M*+H]$^+$, 485.2 (20) [*M*−F]$^+$; elemental analysis calcd (%) for $C_{33}H_{31}BF_2N_2$: C 78.58, H 6.19, N 5.55; found: C 78.41, H 6.09, N 5.47.

1-(3,3-Dimethyl-3-hydroxypropynyl)-6-bromopyrene (2): To a stirred, degassed solution of 1,6-dibromopyrene (1 g, 2.78 mmol) in *n*PrNH$_2$ (150 mL) contained in a Schlenk flask were added [Pd^0(PPh$_3$)$_4$] (0.19 g, 6 % mol), and 2-methylbutyn-2-ol (380 μL, 1.4 equiv). The mixture was stirred at room temperature under argon for five days. The solution was then evaporated to dryness. Chromatography (silica, AcOEt/hexane 30:70) afforded the target compound. Yield: 0.403 g (40 %); ^{1}H NMR ($CDCl_3$, 300 MHz): δ = 8.52 (d, 1H, ^3J = 9.1 Hz), 8.44 (1H, d, ^3J = 9.2 Hz), 8.25 (d, 1H, ^3J = 8.3 Hz), 8.08–8.13 (m, 5H), 1.80 ppm (s, 6H); ^{13}C{^{1}H} NMR ($CDCl_3$, 75 MHz): δ = 132.1, 131.2, 130.63, 130.59, 130.4, 129.9, 128.9, 128.2, 126.8, 126.2, 125.8, 125.7, 125.1, 124.0, 120.7, 118.2, 100.0 (C≡C), 81.0 (C≡C), 66.0, 31.7 ppm; UV/Vis (CH_2Cl_2): λ (ε [M^{-1}cm^{-1}]) = 372 (50100), 352 (35800), 287 (41300), 275 (26200), 249 (49300), 239 (45000) nm; FT-IR (KBr): $\tilde{\nu}$ = 2978 (s), 2143 (C≡C) (s), 1600 (m), 1433 (m), 1268 (m), 1158 (s), 963 (m), 841 (s) cm^{-1}; FAB$^+$/MS (*m*NBA): *m*/*z* (%): 364.03 (80) [*M*+H]$^+$; elemental analysis calcd (%) for $C_{21}H_{15}BrO$: C 69.44, H 4.16; found: C 69.23, H 4.02.

1-(3,3-Dimethyl-3-hydroxypropynyl)-6-triethylsilylacetylenylpyrene (3): To a thoroughly degassed solution of **2** (0.2 g, 0.55 mmol) in *n*PrNH$_2$, was added [Pd^0(PPh$_3$)$_4$] (16 mL, 0.038 g, 6 % mol) and triethylsilylacetylene (150 μL, 0.83 mmol). The mixture was stirred at room temperature under argon until complete consumption of the starting material (16 h). The solution was evaporated and the crude solid was washed twice with water (100 mL) and once with diethyl ether (50 mL). Chromatography on alumina (AcOEt/hexane, gradient from 0:10 to 3:7) afforded the desired compound. Yield: 0.15 g (64 %); ^{1}H NMR ($CDCl_3$, 300 MHz): δ = 8.55 (d, 1H, ^3J = 9.1 Hz), 8.41 (1H, dd, ^3J = 9.1 Hz, ^4J = 1.7 Hz), 8.13 (d, 1H, ^3J = 7.9 Hz), 7.96–8.14 (m, 5H), 1.82 (s, 6H), 1.21 (t, 9H, ^3J = 7.9 Hz), 0.85 ppm (q, 6H, ^3J = 7.9 Hz); ^{13}C{^{1}H} NMR ($CDCl_3$, 75 MHz): δ = 132.2, 131.9, 131.0, 130.9, 130.3, 129.9, 128.1, 127.9, 126.2, 125.9, 124.90, 124.89, 123.9, 118.4, 117.7, 105.2 (C≡C), 99.8 (C≡C), 98.2 (C≡C), 81.1 (C≡C), 66.0, 31.8, 7.7, 4.7 ppm; UV/Vis (CH_2Cl_2): λ (ε [M^{-1}cm^{-1}]) = 390 (76700), 369 (49600), 292 (51600), 281 (27000), 249 (56000), 241 (54000), 230 (47000) nm; FT-IR (KBr): $\tilde{\nu}$ = 2954 (s), 2874 (m), 2144 (C≡C) (s), 1633 (s), 1458 (m), 1161 (m), 972 (m), 843 (s), 738 (s) cm^{-1}; FAB$^+$/MS (*m*NBA): *m*/*z* (%): 423.21 (80) [*M*+H]$^+$; elemental analysis calcd (%) for $C_{25}H_{30}OSi$: C 82.41, H 7.15; found: C 82.17, H 6.98.

1-Ethynyl-6-triethylsilylacetylenylpyrene (4): To solution of **3** (0.370 g, 0.89 mmol) in anhydrous toluene (50 mL) was added NaOH (0.042 mg, 1.01 mmol). The solution was stirred at reflux until total consumption of the starting material (8 h, as checked by TLC). The solution was evaporated and chromatography (silica, AcOEt/hexane 40:60) gave the desired compound. Yield: 0.304 g (90 %); ^{1}H NMR ($CDCl_3$, 200 MHz): δ = 8.56 (d, 1H, ^3J = 9.0 Hz), 8.51 (1H, d, ^3J = 9.0 Hz), 8.15–8.01 (m, 6H), 3.64 (s, 1H), 1.20 (t, 9H, ^3J = 8.1 Hz), 0.86 ppm (q, 6H, ^3J = 8.1 Hz); ^{13}C{^{1}H} NMR ($CDCl_3$, 75 MHz): δ = 132.6, 132.3, 131.5, 131.1, 130.5, 128.3, 128.1, 126.6, 126.1, 125.2, 125.0, 124.0, 123.9, 118.7, 117.2, 105.2, 98.4, 83.0; 82.7, 7.9, 4.8 ppm; UV/Vis (CH_2Cl_2): λ (ε [M^{-1}cm^{-1}]) = 387 (54300), 366 (33300), 348 (14300), 291 (37400), 280 (21000), 249 (46100), 240 (47300), 229 (44200) nm; FT-IR (KBr): $\tilde{\nu}$ = 2955 (s), 2143 (C≡C) (s), 2099 (C≡C) (s), 1603 (m), 1459 (m), 1233 (m), 1016 (s), 843 (s); 719 (s),

646 (m) cm^{-1}; FAB$^+$/MS (*m*NBA): *m*/*z* (%): 365.17 (80) $[M+H]^+$; elemental analysis calcd (%) for $C_{26}H_{24}Si$: C 85.66, H 6.64; found: C 85.35, H 6.32.

General procedure for the ethynyl-linked compounds 6–8: The ethynyl-substituted aromatic compound (1.1 equiv), **5** (1 equiv), $[Pd(PPh_3)_2Cl_2]$ (6% mol), THF and iPr_2NH were mixed in a Schlenk flask. The pink slurry was vigorously degassed with argon. Copper iodide (10% mol) was then added. After stirring for one night at room temperature, the solvent was removed under vacuum. The residue was purified by chromatography on alumina.

4,4-Difluoro-8-(*p*-(ethynyl-4-toluyl)phenyl)-1,3,5,7-tetramethyl-2,4-diethyl-4-bora-3a,4a-diaza-*s*-indacene (6): This was synthesised from compound **5** (0.1 g, 0.20 mmol), tolylacetylene (0.025 g, 0.215 mmol), $[Pd^{II}(PPh_3)_2Cl_2]$ (8.3 mg, 6% mol), THF/iPr_2NH (15:5, 20 mL) and CuI (3.8 mg, 10% mol). Chromatography on (alumina, CH_2Cl_2/hexane 20:80) afforded the pure compound as pink needles. Yield: 0.093 g (95%); ^1H NMR ($CDCl_3$ 200 MHz): δ = 7.47 (AB sys, 4H, *J*(A,B) = 8.1 Hz, $\nu_0\delta$ = 74.3 Hz), 7.33 (AB sys, 4H, *J*(A,B) = 8.1 Hz, $\nu_0\delta$ = 54.5 Hz), 2.54 (s, 6H), 2.31 (q, 4H, ^3J = 7.6 Hz), 1.37 (s, 6H), 0.99 ppm (t, 6H, ^3J = 7.5 Hz); $^{13}C\{^1H\}$ NMR ($CDCl_3$, 100 MHz): δ = 154.4, 139.8, 139.2, 138.6, 136.0, 133.3, 132.6 (CH), 131.9 (CH), 130.9, 129.6 (CH), 128.9 (CH), 124.5, 120.2, 91.2 (C≡C), 88.5 (C≡C), 21.9 (CH_3), 17.5 (CH_2), 14.9 (CH_3), 12.9 (CH_3), 12.3 ppm (CH_3); ^{11}B NMR ($CDCl_3$, 128.38 MHz): δ = 3.86 ppm (t, *J*(B,F) = 32.7 Hz); UV/Vis (CH_2Cl_2): λ (ε[$M^{-1}cm^{-1}$]) = 527 (56100), 357 (9100), 283 (41800), 296 (36400), 253 (65600), 243 (57500) nm; FT-IR (KBr): $\tilde{\nu}$ = 3435 (m), 2964 (m), 22215 (m), 1538 (m), 1474 (s), 1315 (s), 1186 (s), 976 (s), 761 (s) cm^{-1}; FAB$^+$/MS (*m*NBA): *m*/*z* (%): 495.1 (100) $[M+H]^+$, 475.1 (65) $[M-F]$; elemental analysis calcd (%) for $C_{32}H_{33}BF_2N_2$: C 77.74, H 6.73, N 5.67; found: C 77.51, H 6.45, N 5.46.

4,4-Difluoro-8-(*p*-(ethynyl-1-pyrenyl)phenyl)-1,3,5,7-tetramethyl-2,4-diethyl-4-bora-3a,4a-diaza-*s*-indacene (7): This was synthesised from compound **5** (0.094 g, 0.185 mmol), 1-ethynylpyrene (0.042 g, 0.185 mmol), $[Pd^{II}(PPh_3)_2Cl_2]$ (8 mg, 6% mol) in THF/iPr_2NH (15:5 mL) and CuI (4 mg, 10% mol). Chromatography (alumina, CH_2Cl_2/hexane 20:80), followed by recrystallisation (CH_2Cl_2/hexane) gave the titled compound as pink greenish crystals. Yield: 0.096 g (86%); ^1H NMR ($CDCl_3$, 400 MHz): δ = 8.71 (d, 1H, ^3J = 9.0 Hz), 8.27–8.04 (8H, m), 7.62 (AB sys, 4H, *J*(A,B) = 7.9 Hz, $\nu_0\delta$ = 193.7 Hz), 2.58 (s, 6H), 2.34 (q, 4H, ^3J = 7.5 Hz), 1.42 (s, 6H), 1.02 (t, 9H, ^3J = 7.5 Hz), $^{13}C\{^1H\}$ NMR ($CDCl_3$, 100.6 MHz): δ = 154.5, 139.7, 138.7, 136.3, 133.4 (CH), 132.7, 132.4, 131.9, 131.7, 131.5, 131.0, 130.1 (CH), 129.1 (CH), 128.9 (CH), 128.8 (CH), 127.6 (CH), 126.7 (CH), 126.2 (CH), 126.2 (CH), 125.8 (CH), 125.0 (CH), 124.9, 124.7, 124.6, 117.7, 90.4 (C≡C), 94.9 (C≡C), 17.5 (CH_2), 15.0 (CH_3), 12.9 (CH_3), 12.4 (CH_3); ^{11}B NMR ($CDCl_3$, 128.38 MHz): δ = 3.90 (t, *J*(B,F) = 33.2 Hz); UV/Vis (CH_2Cl_2): λ (ε-[$M^{-1}cm^{-1}$]) = 528 (58000), 387 (40000), 370 (44000), 295 (43000), 284 (35000), 240 (48000) nm; FT-IR (KBr): $\tilde{\nu}$ = 3436 (s), 2962 (s), 2142 (m), 1641 (m), 1541 (s), 1474 (s), 1320 (s), 1191 (s), 1072n (s), 979 (s), 848 (s), 713 (s) cm^{-1}; FAB$^+$/MS (*m*NBA): *m*/*z* (%): 605.1 (100) $[M+H]^+$, 585.1(75) $[M-F]$; elemental analysis calcd (%) for $C_{41}H_{35}BF_2N_2$: C 81.46, H 5.84, N 4.63; found: C 81.29, H 5.64, N 4.51.

4,4-Difluoro-8-(*p*-(9-triethylsilylacetylenyl-1-ethynylpyrenyl)phenyl)-1,3,5,7-tetramethyl-2,4-diethyl-4-bora-3a,4a-diaza-*s*-indacene (8): This was synthesised from compound **5** (0.1 g, 0.20 mmol) in THF/iPr_2NH (15:5 mL), $[Pd^{II}(PPh_3)_2Cl_2]$ (8.3 mg, 6% mol), CuI (3.8 mg, 10% mol), and compound **4** (0.075 g, 0.20 mmol). Chromatography (alumina, CH_2Cl_2/hexane 0:1 to 2:8) and recrystallisation from CH_2Cl_2/hexane gave the desired compound as orange-pink needles. Yield: 0.18 g (80%); ^1H NMR ($CDCl_3$ 300 MHz): δ = 8.70 (d, 1H, ^3J = 9.0 Hz), 8.64 (1H, d, ^3J = 9.2 Hz), 8.13–8.26 (m, 6H), 7.85 (d, 2H, ^3J = 8.3 Hz), 7.38 (d, 2H, ^3J = 8.3 Hz), 2.56 (s, 6H), 2.33 (q, 4H, ^3J = 7.5 Hz), 1.40 (s, 6H), 1.17 (t, 9H, ^3J = 7.8 Hz), 1.00 (6H, t, ^3J = 7.5 Hz), 0.83 (q, 6H, ^3J = 7.9 Hz); $^{13}C\{^1H\}$ NMR ($CDCl_3$, 75 MHz): δ = 154.2, 139.4, 138.4, 136.1, 133.1 (CH), 132.5, 132.4, 132.2, 131.5, 131.3, 130.7, 130.6 (CH), 130.1 (CH), 128.7 (CH), 128.5 (CH), 128.3 (CH), 126.7 (CH), 126.3 (CH), 125.3 (CH), 125.2 (CH), 124.3, 124.2, 124.1, 118.9, 118.1, 105.1 (C≡C), 96.7 (C≡C), 94.9 (C≡C), 89.9 (C≡C), 17.2 (CH_2), 14.8 (CH_3), 12.7 (CH_3), 12.1 (CH_3), 7.7 (CH_3), 4.6 (CH_2); ^{11}B NMR ($CDCl_3$, 128.38 MHz): δ = 3.89 (t, *J*(B,F) = 32.6 Hz); UV/Vis (CH_2Cl_2): λ (ε[$M^{-1}cm^{-1}$]) = 529 (68800), 413 (68200), 391 (64400), 296 (36400), 253 (65600), 243 (57500) nm; FT-IR (KBr): $\tilde{\nu}$ = 2872 (m), 2142 (m), 1540 (s), 1321 (m), 1191 (m), 1150 (m), 980 (m), 842 (m), 738 (m) cm^{-1}; FAB$^+$/MS (*m*NBA): *m*/*z* (%): 743.1 (80) $[M+H]^+$; elemental analysis calcd (%) for $C_{49}H_{49}BF_2N_2Si$: C 79.23, H 6.65, N 3.77; found: C 78.91, H 6.37, N 3.56.

4,4-Difluoro-8-(*p*-(9-acetylenyl-1-ethynylpyrenyl)phenyl)-1,3,5,7-tetramethyl-2,4-diethyl-4-bora-3a,4a-diaza-*s*-indacene (9): To a stirred solution of compound **8** (0.054 g, 0.073 mmol) in CH_2Cl_2/methanol (20 mL, 1:1) was added K_2CO_3 (0.1 g, 0.7 mmol). After complete consumption of the starting material (2 d), the solution was concentrated by rotary evaporation, and the crude product was purified by column chromatography (alumina, hexane/CH_2Cl_2 70:30). Recrystallisation from CH_2Cl_2/hexane gave **8** as pink crystals. Yield: 32 mg (67%); ^1H NMR ($CDCl_3$, 400 MHz): δ = 8.73 (d, 1H, ^3J = 9.0 Hz), 8.64 (1H, d, ^3J = 9.0 Hz), 8.26 (d, 1H, ^3J = 7.5 Hz), 8.18–8.24 (m, 5H), 7.85 (d, 2H, ^3J = 8.0 Hz), 7.38 (d, 2H, ^3J = 8.0 Hz), 3.66 (s, 1H), 2.56 (s, 6H), 2.33 (q, 4H, ^3J = 7.5 Hz), 1.40 (s, 6H), 1.00 (t, 6H, ^3J = 7.5 Hz); $^{13}C\{^1H\}$ NMR ($CDCl_3$, 100 MHz): δ = 154.2, 139.4, 138.4, 136.2, 133.1, 132.8 (CH), 132.5, 132.2, 131.6, 131.5, 130.8 (CH), 130.2 (CH), 128.9 (CH), 128.5 (CH), 128.4 (CH), 126.6 (CH), 126.4 (CH), 125.5 (CH), 125.3 (CH), 124.3, 124.2, 124.1, 118.3, 117.5, 95.1 (C≡C), 89.9 (C≡C), 83.3 (C≡CH), 82.7 (C≡C), 17.3 (CH_2), 14.8 (CH_3), 12.7 (CH_3), 12.1 (CH_3); ^{11}B NMR ($CDCl_3$, 128.38 MHz): δ = 3.89 (t, *J*(B,F) = 33.5 Hz); UV/Vis (CH_2Cl_2): λ (ε[$M^{-1}cm^{-1}$]) = 527 (66300), 408 (59000), 386 (57600), 292 (46400), 248 (72200) nm; FT-IR (KBr): $\tilde{\nu}$ = 3436 (m), 2142 (m), 1603 (m), 1539 (s), 1475 (m), 1320 (m), 1191 (s), 1150 (m), 979 (m), 846 (m), 762 (m) cm^{-1}; FAB$^+$/MS (*m*NBA): *m*/*z* (%): 609.1 (100) $[M-F]^+$; elemental analysis calcd (%) for $C_{43}H_{35}BF_2N_2$: C 82.17, H 5.61, N 4.46; found: C 82.37, H 5.42, N 4.19.

4,4-Difluoro-8-(*p*-(9-(1-acetylenylpyrenyl)-1-ethynylpyrenyl)phenyl)-1,3,5,7-tetramethyl-2,4-diethyl-4-bora-3a,4a-diaza-*s*-indacene (10): To a stirred, degassed solution of **9** (20 mg, 0.032 mmol) in benzene/iPr_2NH (3 mL, 3:1) contained in a Schlenk flask were added progressively $[Pd^0(PPh_3)_4]$ (1.1 mg, 6% mol) and 1-bromopyrene (13.5 mg, 0.048 mmol). The mixture was stirred at room temperature under argon until starting material had been completely consumed (16 h). The solution was then evaporated, and the crude precipitate was washed with water (2×) and diethyl ether (1×). Column chromatography (alumina, CH_2Cl_2/hexane gradient from 0:100 to 20:80) and recrystallisation from CH_2Cl_2/hexane afforded the target compound as pink needles. Yield: 25 mg (95%); ^1H NMR ($CDCl_3$, 300 MHz): δ = 8.96 (d, 1H, ^3J = 9.0 Hz), 8.91 (1H, d, ^3J = 9.0 Hz), 8.77 (d, 1H, ^3J = 9.0 Hz), 8.44 (d, 1H, ^3J = 8.0 Hz), 8.41 (d, 1H, ^3J = 8.5 Hz), 8.31–8.21 (m, 9H), 8.17–8.04 (m, 3H), 7.87 (d, 2H, ^3J = 8.3 Hz), 7.39 (d, 2H, ^3J = 8.3 Hz), 2.58 (s, 6H), 2.36 (q, 4H, ^3J = 7.5 Hz), 1.43 (s, 6H), 1.00 (t, 6H, ^3J = 7.5 Hz); $^{13}C\{^1H\}$ NMR ($CDCl_3$, 75 MHz): δ = 154.3, 142.5, 139.4, 138.44, 138.42, 136.2, 133.1, 132.5, 132.3 (CH), 132.21, 132.15, 131.6, 131.5, 131.4, 130.8, 130.4, 130.3 (CH), 130.0 (CH), 129.9 (CH), 128.9 (CH), 128.8 (CH), 128.54 (CH), 128.50 (CH), 127.5 (CH), 126.8 (CH), 126.5 (CH), 126.4 (CH), 125.9 (CH), 125.8 (CH),125.6 (CH), 125.5 (CH), 125.4 (CH), 124.6 (CH), 124.52, 124.51, 124.2, 124.1, 118.2, 118.0, 95.2 (C≡C), 95.0 (C≡C), 94.4 (C≡CH), 81.2 (C≡C), 17.2 (CH_2), 14.8 (CH_3), 12.7 (CH_3), 12.1 (CH_3); ^{11}B NMR ($CDCl_3$, 128.38 MHz): δ = 3.89 (t, *J*(B,F) = 33.0 Hz); UV/Vis (CH_2Cl_2): λ (ε[$M^{-1}cm^{-1}$]) = 532 (52900), 458 (57600), 430 (57000), 367 (24900), 304 (32600), 289 (34800) 247 (43900) nm; FT-IR (KBr): $\tilde{\nu}$ = 2141 (m), 2029 (m), 1403 (s), 1315 (m), 1188 (m), 1116 (m), 977 (m), 8432 (m), 761 (m) cm^{-1}; FAB$^+$/MS (*m*NBA): *m*/*z* (%): 829.2 (80) $[M+H]^+$, 809.1 (100) $[M-F]^+$; elemental analysis calcd (%) for $C_{59}H_{43}BF_2N_2$: C 85.50, H 5.23, N 3.38; found: C 85.41, H 5.00, N 3.07.

Acknowledgements

This work was supported by the CNRS, the EPSRC, the Université Louis Pasteur, the University of Newcastle, and IST/ILO Contract 2001–33057.

[1] K. Van Dyke, C. Van Dyke, K. Woodfork in *Luminescence Biotechnology: Instruments and Applications*, CRC Press, Boca Raton, Fl, USA, **2002**.
[2] B. Valeur in *Molecular Fluorescence: Principles and Applications*, Wiley-VCH, Weinheim, Germany, **2002**.
[3] Th. Forster, *Discuss. Faraday Soc.* **1959**, *27*, 7–21.
[4] D. L. Dexter, *J. Chem. Phys.* **1953**, *21*, 836.
[5] S. Speiser, *Chem. Rev.* **1996**, *96*, 1953.
[6] R. P Haugland, *Handbook of Molecular Probes and Research Products*, Ninth Edition; Molecular Probes, Inc., Eugene, OR, USA, **2002**.
[7] A. Burghart, H. Kim, M. B. Wech, . L. H. Thorensen, J. Reibenspies, K. Burgess, *J. Org. Chem.* **1999**, *64*, 7813.
[8] L. H. Thoresen, H. Kim, M. B. Welch, A. Burghart, K. Burgess, *Synlett* **1998**, 1276.
[9] T. Chen, J. H. Boyer, M. L. Trudell, *Heteroat. Chem.* **1997**, *8*, 51.
[10] G. Sathyamoorthi, L. T. Wolford, A. M. Haag, J. H. Boyer, *Heteroat. Chem.* **1994**, *5*, 245.
[11] T. Gareis, C. Huber, O. S. Wolfbeis, J. Daub, *Chem. Commun.* **1997**, 1717.
[12] M. Kollmannsberger, K. Rurack, U. Resch-Genger, J. Daub, *J. Phys. Chem.* **1998**, *102*, 10211.
[13] K. Rurack, M. Kollmannsberger, U. Resch-Genger, J. Daub, *J. Am. Chem. Soc.* **2000**, *122*, 968.
[14] B. Turfan, E. U. Akkaya, *Org. Let.* **2002**, *4*, 2857.
[15] C. Goze, G. Ulrich, L. Charbonnière, R. Ziessel, *Chem. Eur. J.* **2003**, *9*, 3748.
[16] F. Li, S. I. Yang, Y. Ciringh, J. Seth, C. H. Martin, III, D. L. Singh, D. Kim, R. R. Birge, D. F. Bocian, D. Holten, J. S. Lindsey, *J. Am. Chem. Soc.* **1998**, *120*, 10001.
[17] A. Burghart, L. H. Thorese, J. Che, K. Burgess, F. Bergström, L. B-Å Johansson, *Chem. Commun.* **2000**, 2203.
[18] C.-W. Wan, A. Burghart, J. Chen, F. Bergström, L. B.-A. Johanson, M. F. Wolford, T. G. Kim, M. R. Topp, R. M. Hochstrasser, K. Burgess, *Chem. Eur. J.* **2003**, *9*, 4430.
[19] A. Harriman, M. Hissler, A. Khatyr, R. Ziessel, *Chem. Commun.* **1999**, 735–736.
[20] A. Harriman, M. Hissler, A. Khatyr, R. Ziessel, *Eur. J. Inorg. Chem.* **2003**, 955; A. Harriman, A. Khatyr, R. Ziessel, *Dalton Trans.* **2003**, 2061.
[21] H. Fischer, P. Halbig, B. Walach, *Ann. Chem.* **1927**, *452*, 268.
[22] M. Hissler, A. Harriman, A. Khatyr, R. Ziessel, *Chem. Eur. J.* **1999**, *5*, 3366; Z. Shen, R. Procházka, J. Daub, N. Fritz, N. Acar, S. Schneider, *Phys. Chem. Chem. Phys.* **2003**, *5*, 3257.
[23] J. Grimshaw, J. Trocha-Grimshaw, *J. Chem. Soc. Perkin 1*, **1972**, 1622.
[24] C. Goze, D. V. Kozlov, F. N. Castellano, J. Suffert, R. Ziessel, *Tetrahedron Lett.* **2003**, *44*, 8713.
[25] G. Ulrich, R. Ziessel, *Synlett* **2004**, 439. G. Ulrich, R. Ziessel, *J. Org. Chem.* **2004**, *69*, 2070; G. Ulrich, R. Ziessel, *Tetrahedron Lett.* **2004**, *45*, 1949.
[26] V. R. Thalladi, H.-C. Weiss, D. Bläser, R. Boese, A. Nangia, G. R. Desiraju, *J. Am. Chem. Soc.* **1998**, *120*, 8702.
[27] Z. Shen, H. Röhr, K. Rurack, H. Uno, M. Spieles, B. Schulz, G. Reck, N. Ono, *Chem. Eur. J.* **2004**, *10*, 4853.
[28] J. Karolin, L. B.-A. Johansson, L. Strandberg, T. Ny, *J. Am. Chem. Soc.* **1994**, *116*, 7801; P. Toele. H. Zhang, C. Trieflinger, J. Daub, M. Glasbeek, *Chem. Phys. Lett.* **2003**, *368*, 66.
[29] A. Harriman, M. Hissler, R. Ziessel, *Phys. Chem. Chem. Phys.* **1999**, *1*, 4203.
[30] K. Rurack, M. Kollmannsberger, U. Resch-Genger, J. Daub, *J. Am. Chem. Soc.* **2000**, *122*, 968.
[31] K. Rurack, M. Kollmannsberger, J. Daub, *Angew. Chem.* **2001**, *113*, 396; *Angew. Chem. Int. Ed.* **2001**, *40*, 385; .
[32] M. Kollmannsberger, K. Rurack, U. Resch-Genger, J. Daub, *J. Phys. Chem. A* **1998**, *102*, 10211.
[33] R. Englman, J. Jortner, *Mol. Phys.* **1970**, *18*, 145.
[34] T. Förster, *Discuss. Faraday Soc.* 1959, 27, 7.
[35] V. Grosshenny, A. Harriman. M. Hissler, R. Ziessel, *J. Chem. Soc. Faraday Trans.* **1996**, *92*, 2223.
[36] J. Olmsted, III, *J. Phys. Chem.* **1979**, *83*, 2581.
[37] R. Leutz, A. Suzuki, A. Akisawa, T. Kashiwagi, *J. Opt. A* **2000**, *2*, 112.
[38] T. L. Netzel, *J. Biol. Inorg. Chem.* **1998**, *3*, 210.
[39] O. Dangles, F. Guibe, G. Balavoine, *J. Org. Chem.* **1987**, *52*, 4984.
[40] D. R. Coulson, *Inorg. Synth.* **1972**, *13*, 121.
[41] Z. Otwinovski and W. Minor, Macromolecular Crystallography, Part A in *Methods in Enzymology*, Academic Press **1997**, 307–326.
[42] G. M. Sheldrick, SHELX97, Program for the Refinement of Crystal Structures from Diffraction Data, University of Göttingen, Germany, **1997**.

Received: April 4, 2005
Published online: September 20, 2005

